



**Processing Seismic Ambient Noise Data with the Continuous
Wavelet Transform to Obtain Reliable Empirical Green's
Functions**

Journal:	<i>Geophysical Journal International</i>
Manuscript ID	GJI-S-19-0746
Manuscript Type:	Research Paper
Date Submitted by the Author:	18-Aug-2019
Complete List of Authors:	Yang, Yang; University of Memphis, Center for Earthquake Research and Information Liu, Chunyu; University of Memphis, Center for Earthquake Research and Information Langston, Charles; University of Memphis, Center for Earthquake Research and Information
Keywords:	Seismic interferometry < SEISMOLOGY, Seismic noise < SEISMOLOGY, Wavelet transform < GEOPHYSICAL METHODS

Processing Seismic Ambient Noise Data with the CWT

1
2
3 1 Processing Seismic Ambient Noise Data with the Continuous Wavelet Transform to Obtain
4 2 Reliable Empirical Green's Functions

5 3
6 4
7 4 Yang Yang¹

8 5
9 6 Chunyu Liu¹

10 7
11 8 Charles A. Langston¹

12 9
13 10
14 10 ¹Center for Earthquake Research and Information

15 11 University of Memphis

16 12 3876 Central Ave., Suite 1

17 13 Memphis, TN 38152

18 14
19 15 Submitted to the

20 16 *Geophysical Journal International*

21 17 on August 17, 2019

22 18
23 19 Running title: Processing Seismic Ambient Noise Data with the CWT

24 20
25 21
26 21 Yang.Yang@memphis.edu

27 22
28 23 cliu5@memphis.edu

29 24
30 25
31 26
32 27
33 28
34 29
35 30
36 31
37 32
38 33
39 34
40 35
41 36
42 37
43 38
44 39
45 40
46 41
47 42
48 43
49 44
50 45
51 46
52 47
53 48
54 49
55 50
56 51
57 52
58 53
59 54
60 55

35 23 clangstn@memphis.edu

*Processing Seismic Ambient Noise Data with the CWT***SUMMARY**

We propose a new data processing flow to compute empirical Green's functions (EGF) from ambient seismic noise based on a soft thresholding designating and denoising method using the continuous wavelet transform. The designating algorithm is carried out during the initial data processing to remove earthquakes and other transient signals in the seismic record. A continuous wavelet transform denoising algorithm removes the noise in the final stacked cross-correlogram. The overall data processing procedure is divided into four stages: (1) single station data preparation, (2) remove earthquakes and other signals in the seismic record, (3) spectrum whitening, cross-correlation and temporal stacking, (4) remove the noise in the stacked cross-correlogram to deliver the final EGF. The whole process is automated to make it accessible for large datasets. Synthetic data constructed with a recorded earthquake and recorded ambient noise is used to test the designating method. We then apply the new processing flow to data recorded by the USArray Transportable Array stations near the New Madrid Seismic Zone where many seismic events and transient signals are observed in the data. We compare the EGFs calculated from our new flow with time domain normalization and our results show improved signal-to-noise ratios and deliver more reliable measurements that can be used for further processing. The designating method improves the homogeneity of the ambient noise wavefield which is an intrinsic requirement for seismic interferometry. The final denoising step suppresses random noise and provides clearer EGFs for the next processing step.

Keywords: Seismic interferometry, seismic noise, wavelet transform

INTRODUCTION

Cross-correlation of diffuse wave fields, such as from ambient noise or scattered coda waves, can be used to estimate the medium Green's function termed the empirical Green's function (EGF) between a pair of stations (e.g. Shapiro et al. 2005; Sabra et al. 2005; Wapenaar & Fokkema 2006). This method has been widely applied to data collected in different regions over the past 15 years to extract surface waves and body waves. Densely deployed networks have provided an opportunity for high-resolution surface wave tomography (e.g. Yao et al. 2006; Lin et al. 2008; Bensen et al. 2008) and full waveform inversion (e.g. Gao & Shen 2014; Emry et al. 2018). In spite of these applications, there have been fewer efforts to develop improved ambient noise data processing procedures in order to acquire more reliable and higher signal-to-noise ratio (SNR) EGFs. Bensen et al. (2007) summarized and compared different procedures on the use of seismic records to obtain surface wave dispersion measurements and their suggestions are still the main procedures that are generally used today to process ambient noise data.

Ground motion produced by earthquakes and other sources, such as non-stationary noise sources near a station or weather storm signals, will be recorded on the seismogram and are often considered as "useful signals" that contain important information about the seismic source and underground structure. However, in ambient noise tomography, these signals destroy the diffuse wave field assumption and need to be considered as "noise" in correlation processing. One of the most important steps during the processing is to remove these signals to obtain as "pure" ambient noise as possible. In Bensen et al. (2007), this step is called "time-domain normalization" or "temporal normalization", which is a procedure for reducing the effect of earthquakes, instrumental irregularities and non-stationary noise sources near to stations on the cross-correlations. This process balances the amplitude of ambient noise relative to the amplitude of

Processing Seismic Ambient Noise Data with the CWT

1
2
3 69 unwanted signals. Here, “signal” and “noise” are related to what is being studied and depend on
4
5 70 whether removing “signal” or “noise” is useful for our purpose. Earthquakes and other source
6
7 71 “signals” should be removed before cross-correlation because large amplitude signals at zero-
8
9 72 delay time in the cross-correlation disguise the surface wave arrival from the microseisms. To
10
11 73 avoid confusion, based on the common way of naming “ambient noise”, we call the removing of
12
13 74 earthquakes and other non-stationary noise source “signals” as designaling in this paper although
14
15 75 the mathematics of doing so is the same as denoising.
16
17
18

19 76 Bensen et al. (2007) summarized different methods for identifying and removing
20
21 77 earthquakes and other contaminants from the original recordings. These include 1-bit
22
23 78 normalization, running absolute mean normalization and water level normalization that all
24
25 79 suppress the contaminating signals. However, amplitude information is not fully retained in the
26
27 80 cross-correlation because of the inherent amplitude down-weighting process in these methods.
28
29 81 Amplitude is of fundamental importance for body wave anelastic attenuation estimation and
30
31 82 basement resonance estimation based on the horizontal to vertical amplitude ratio (H/V ratio) of
32
33 83 surface waves. Bensen et al. (2007) also suggested using running absolute mean normalization as
34
35 84 the best practice to process the ambient noise data. In the rest of this paper, we will call this
36
37 85 method as “time domain normalization” and it will be used as the benchmark method for
38
39 86 comparison.
40
41
42
43

44 87 Removing transient signals while not touching the ambient noise itself is a crucial
45
46 88 requirement for successful ambient noise data processing. We propose a method based on the
47
48 89 Continuous Wavelet Transform (CWT) for dealing with this problem. The CWT has been widely
49
50 90 used to for seismic analysis and denoising purposes (Pazos et al. 2003; Chik et al. 2009; To et al.
51
52 91 2009; Ansari et al. 2010; Beenamol et al. 2012; Mousavi & Langston 2016; Mousavi et al. 2016).
53
54
55
56
57
58
59
60

Processing Seismic Ambient Noise Data with the CWT

1
2
3 92 Compared with other denoising methods, using the CWT to achieve denoising has many natural
4
5 93 translation-invariant and time-frequency properties such as reducing pseudo-Gibbs artifacts in
6
7 94 the denoised signal (Elad & Aharon, 2006). In ambient noise data, the noise record usually
8
9
10 95 dominates the time series with earthquakes or other transient signals contaminating only a small
11
12 96 portion of the whole record. The statistical properties of the ambient noise can be estimated
13
14 97 based on a segment of the noise record and time-frequency CWT analysis allows us to navigate
15
16
17 98 the rest of data and remove the unwanted signals. The CWT provides one of the best choices for
18
19 99 ambient noise designating. Unlike its normal purpose for removing noise, we use this method in
20
21
22 100 a reverse manner to take the signal out and keep the background ambient noise.

23
24 101 The motivation of this paper is to introduce a designating procedure based on the CWT
25
26 102 and apply it to ambient noise data processing. We also use essentially the same method to
27
28 103 remove noise in the final stacked cross-correlograms. Details of the designating and denoising
29
30
31 104 methods will be given and then explored using a synthetic data example. Next, we use our new
32
33 105 ambient noise processing flow to process data collected from EarthScope's USArray
34
35 106 Transportable Array within the northern Mississippi embayment. The New Madrid Seismic Zone
36
37 107 (NMSZ) inside of the Mississippi embayment is one of the most earthquake-active intraplate
38
39
40 108 regions in North America (Hildenbrand, 1985; Cox et al., 2001; Tuttle et al., 2002; Thomas,
41
42 109 2006; Van Arsdale et al., 2007; Powell et al., 2010; Dunn et al., 2013; Van Arsdale and Cupples,
43
44
45 110 2013; Nyamwandha et al., 2016; Yang & Langston, 2019). Abundance of seismic events in the
46
47 111 NMSZ could be used to test the efficiency and robustness of our method. Using the real data, the
48
49 112 resulting EGFs and the final dispersion curves obtained from our method and Bensen's method
50
51
52 113 are compared.

53
54 114

115 CWT DENOISING AND DESIGNALING

116 CWT

117 The CWT (Daubechies 1992) is a popular tool to study time-frequency representations of
 118 continuous or discrete time series. This mathematical transformation decomposes a signal into
 119 different scales as a function of time. Different scales provide different resolutions (or can be
 120 considered as different pseudo-frequency components) of the original signal. From this point of
 121 view, it provides better resolution compared to the short time Fourier transform (Tary et al.
 122 2014). Assuming we have a time series $s(t)$, for a given mother wavelet $\psi(t)$, the CWT of time
 123 series $s(t)$ at scale a ($a > 0$) and time shift b can be expressed as (Daubechies 1992)

$$124 \quad Ws(a, b) = \int_{-\infty}^{+\infty} s(t) a^{-1/2} \psi^* \left(\frac{t-b}{a} \right) dt, \quad (1)$$

125 where the $*$ indicates the complex conjugate and $Ws(a, b)$ is the wavelet coefficient
 126 representation of the signal $s(t)$ at scale a and time shift b . The Fourier transform of the mother
 wavelet $\psi(t)$ should satisfy the admissibility condition (Daubechies 1992; Farge 1992)

$$127 \quad 0 < C_\psi = \int_{-\infty}^{+\infty} |\omega|^{-1} |\hat{\psi}(\omega)|^2 d\omega < \infty, \quad (2)$$

128 in which $\hat{\psi}(\omega)$ is the Fourier transform of the mother wavelet $\psi(t)$ and C_ψ is called the wavelet
 129 admissibility constant. Such a wavelet is called an admissible wavelet. An admissible wavelet
 also implies that $\hat{\psi}(0) = 0$ so that the integration over time must be zero (Daubechies 1992). To
 130 recover the original signal from the CWT representations, the inverse CWT can be expressed as

$$131 \quad s(t) = \frac{1}{C_\psi} \int_0^\infty \int_{-\infty}^{+\infty} \frac{1}{\sqrt{a}} Ws(a, b) \psi \left(\frac{t-b}{a} \right) \frac{dad b}{a^2}. \quad (3)$$

132 The CWT of a discrete time series can be expressed in the similar way by replacing
 integration with summation (Torrence & Compo 1998) and different fast algorithms are

1
2
3 133 developed to make it computation affordable (Rioul & Duhamel 1992). In another mathematical
4
5 134 view of equation (1), the CWT can be considered as a cross-correlation of the target time series
6
7
8 135 $s(t)$ with different wavelets that are stretched or compressed and shifted versions of the selected
9
10 136 mother wavelet $\psi(t)$. Because of this cross-correlation property, the CWT can be calculated
11
12 137 using the fast Fourier transform (FFT) in the frequency domain (Daubechies 1992). The CWT
13
14 138 spectrum $Ws(a, b)$ for the time series $s(t)$ is the time-frequency decomposition of the original
15
16 139 signal, with different scales a analogous to wave period (inverse frequency) and b indicating
17
18
19 140 time lag.
20
21

22 141

24 142 **Designing and denoising via soft thresholding**

26 143 Langston & Mousavi (2019) discussed an efficient method based on the CWT to denoise
27
28 144 or designal a time series using the statistical estimation of the noise. In this study, we implement
29
30 145 the soft thresholding method in the ambient noise data processing flow. Essentially, the noise is
31
32 146 estimated and then removed for different scales of wavelets by a less severe manner. The size of
33
34 147 datasets used for ambient noise tomography is usually very large. Thus, processing ambient
35
36 148 noise data requires an algorithm that is not time-consuming and works efficiently. Soft
37
38 149 thresholding (Weaver et al., 1991) can remove noise efficiently compared to computationally
39
40 150 intensive block thresholding algorithms on the wavelet scale-time plane (Mousavi & Langston,
41
42 151 2016).
43
44
45

47 152 In order to apply the CWT soft thresholding denoising, the original time series $s(t)$ is
48
49 153 first transformed into the CWT time-frequency domain to get the CWT spectrum $Ws(a, b)$. The
50
51 154 noise level for a specific scale a is estimated and the CWT coefficients for this scale are
52
53
54 155 modified by the non-linear soft thresholding given by
55
56
57
58
59
60

Processing Seismic Ambient Noise Data with the CWT

$$\bar{W}s(a, b) = \begin{cases} \text{sign}[W_s(a, b)](\|W_s(a, b)\| - \beta(a)) & \text{if } \|W_s(a, b)\| \geq \beta(a), \\ 0 & \text{otherwise} \end{cases}, \quad (4)$$

156 where

$$\text{sign}[W_s(a, b)] = \frac{W_s(a, b)}{\|W_s(a, b)\|}, \quad (5)$$

157 $\bar{W}s(a, b)$ is the CWT spectrum after denoising for the scale a and $\|\cdot\|$ stands for the modulus of
 158 the complex spectrum in the CWT domain. The threshold function $\beta(a)$ is determined based on
 159 the statistics of the absolute value of the noise for scale a . If the CWT spectrum is less than
 160 $\beta(a)$, it is considered as the noise and we will remove it by setting it to zero. Otherwise, it
 161 contains both noise and signal, and the predefined noise is subtracted from the original spectrum.
 162 This criterion is applied to data at each scale in the CWT spectrum. Ambient noise data is
 163 continuously recorded and earthquakes and other signals only make up a small proportion of the
 164 whole record. The noise level $\beta(a)$ can be well estimated with a predetermined time segment
 165 which contains only ambient noise. Much of the signal processing procedures start from an
 166 assumption of Gaussian noise. The threshold function can be computed using the mean and
 167 standard deviation of the CWT spectrum for scale a within the selected time segment:

$$\beta(a) = \text{mean}(\|W_s(a, b)\|) + N \text{std}(\|W_s(a, b)\|), \quad (6)$$

168 where

$$\text{mean}(\|W_s(a, b)\|) = \frac{1}{T_2 - T_1} \int_{T_1}^{T_2} \|W_s(a, b)\| db, \quad (7)$$

$$\text{std}(\|W_s(a, b)\|) = \left[\frac{1}{T_2 - T_1} \int_{T_1}^{T_2} (\|W_s(a, b)\| - \text{mean}(\|W_s(a, b)\|))^2 db \right]^{\frac{1}{2}}, \quad (8)$$

169 and N is a parameter that controls the threshold noise level. The time limits T_1 and T_2 represent
 170 the start and end time of the selected time segment.

Processing Seismic Ambient Noise Data with the CWT

1
2
3 171 There are different criteria to choose the threshold coefficient, N , in equation (6). Simply
4
5 172 choosing $N = 3$ will yield a signal at 99.7% confidence level (Starck et al., 2010) if the CWT
6
7 173 coefficients of the noise follow a normal distribution. This method is straightforward to estimate
8
9 174 the noise level. But unfortunately, the assumption that the CWT coefficients follow a Gaussian
10
11 175 distribution is rarely seen in seismic noise data (Langston & Mousavi, 2019). The distribution for
12
13 176 real ambient noise is usually unpredictable. However, we can estimate a data-driven noise level
14
15 177 by taking the approach of empirically estimating the cumulative distribution of noise and then
16
17 178 calculating the 99% confidence value for the distribution. To calculate the empirical cumulative
18
19 179 distribution function (ECDF), we can order the N samples noise values and then assign a
20
21 180 probability jump of $1/N$ when a value is attained, starting with the smallest value. Thus, the
22
23 181 threshold function becomes:

$$\beta(a) = \text{ECDF}^{-1}(P = 0.99), \quad (9)$$

24
25
26
27
28
29
30
31
32 182 where ECDF^{-1} is the inverse of the cumulative distribution function or the quantile.

33
34 183 In Fig. 1, we compare the threshold functions assuming Gaussian statistics in equation (6) Fig.1
35
36 184 and non-Gaussian statistics in equation (9). The distribution of the empirical probability
37
38 185 distribution function of the real noise is different compared to a Gaussian distribution and gives
39
40 186 quite different estimated noise levels. Overall, there are significant differences between the
41
42 187 ECDF and Gaussian threshold functions. It also suggests that the ECDF method would lead to a
43
44 188 better estimate of the threshold and thus we use the ECDF method to estimate the noise level in
45
46 189 our processing.

47
48
49
50 190 Designating reverses the denoising process. This procedure can be applied in our ambient
51
52 191 noise processing to remove earthquakes and other signals. For the soft thresholding case, signal
53
54 192 is removed by using

Processing Seismic Ambient Noise Data with the CWT

$$\bar{W}_s(a, b) = \begin{cases} \text{sign}[W_s(a, b)]\beta(a) & \text{if } \|W_s(a, b)\| \geq \beta(a) \\ W_s(a, b) & \text{otherwise} \end{cases}. \quad (10)$$

193 At each scale, if the CWT spectrum is less than the estimated noise level, we consider it as the
 194 noise and keep the spectrum. Otherwise, we consider it as the signal and remove it by setting the
 195 coefficient to the noise level.

196 Using the soft thresholding method to remove noise or signal based on ECDF is very
 197 straightforward and efficient. After applying equation (4) for denoising or equation (10) for
 198 designating, we get our new CWT spectrum and get the final denoised or designated output for
 199 our next processing step by doing the inverse CWT from equation (3).

200

DATA AND DATA PROCESSING FLOW

201

Data preprocessing

202

203 We use data from 55 broadband seismic stations of EarthScope's USArray Transportable
 204 Array (TA) recorded during July, 2012, within and around the northern Mississippi embayment
 205 (Fig. 2) to demonstrate our ambient noise data processing flow. Velocity models for this area are
 206 developed using full waveform tomography of the EGFs extracted from all temporary and
 207 permanent stations. The crustal and upper mantle structures underneath the northern Mississippi
 208 embayment are investigated. These models will be the subject of future reports.

209 In order to compare the robustness of our method, we compare cross-correlations and
 210 dispersion curves with those computed based on time domain normalization (TDN). The
 211 "MSNoise" package (Lecocq et al., 2014) is a python package which implements the TDN
 212 method.

213 We first download daily vertical component waveform data for each station through the
 214 IRIS (www.iris.edu) FDSN web service and work with them in SAC format, remove the

Fig.2

Processing Seismic Ambient Noise Data with the CWT

1
2
3 215 instrument response, remove the mean and trend, apply a bandpass filter from 0.02Hz to 1Hz and
4
5 216 downsample the sampling rate from 40Hz to a 5Hz. The reason why we choose the passband
6
7 217 0.02-1Hz is that previous studies (e.g. Liang et al., 2008; Langston et al., 2009; Liu et al., 2018a;
8
9 218 Yang & Langston, 2019) observed prominent surface wave arrivals in this frequency band.
10
11
12 219 Downsampling the sampling rate to 5 Hz not only reduces the storage but also reduces the
13
14 220 computation time of cross-correlations. Small events are usually higher frequency and are
15
16 221 filtered out during the downsampling.
17
18
19 222
20
21

223 CWT ambient noise data processing flow

22 224 The temporal normalization step is replaced by the designating method described above.
23
24 225 After single station data preparation, the CWT designating method is applied on each day of the
25
26 226 data, followed by spectral whitening to provide spectrum-balanced data. A 5% taper is applied at
27
28 227 the beginning and end of each data segment to avoid artifacts during cross-correlation. Each pair
29
30 228 of stations are then cross-correlated and all one-day cross-correlograms for the month are stacked
31
32 229 to increase the SNR.
33
34
35
36

37 230 In order to estimate the noise statistics for each day, we need to find a segment of the data
38
39 231 that only contains noise. This is realized by a simple algorithm. For each day's data, we divide
40
41 232 the time series into 48 half hour segments. The maximum absolute value in each segment is
42
43 233 determined and the segment with the minimum absolute value is chosen to estimate noise
44
45 234 statistics. There is no guarantee that earthquakes or other signals will not appear within the
46
47 235 selected segment, but it provides a fast and accurate way to find this estimate. The time duration
48
49 236 for each segment could be shorter when teleseismic events occur more frequently but each
50
51
52
53
54
55
56
57
58
59
60

Processing Seismic Ambient Noise Data with the CWT

1
2
3 237 segment still needs to be long enough to make a robust estimate. The test in Fig. 2 shows that the
4
5 238 noise level could be estimated accurately with data time series as short as 500 seconds.

7 239 Besides removing the signal, soft thresholding can also be used to remove the noise in the
8
9
10 240 final stacked EGFs to increase the SNR (equation 4). This step is applied to deliver the final
11
12 241 EGFs.

14 242 Our new ambient noise data processing flow can be summarized into the following steps:

17 243 Step 1: Pre-processing: prepare waveform data for each station individually, which
18
19 244 includes cutting the data into intervals of one-day, removing the instrument response, removing
20
21 245 the mean and trend, applying a bandpass filter and resampling the data to a 5Hz sampling rate.

23 246 Step 2: Designal: for each one-day time series for a station, apply the soft thresholding
24
25 247 designaling method to remove earthquakes and other transients.

28 248 Step 3: Spectral whitening, cross-correlation and stack: applying spectral whitening for
29
30 249 each one-day time series for a station to provide a broader-band and spectrum-balanced data.
31
32 250 Calculate the cross-correlation for each possible day and each station pair. Stack the desired
33
34 251 number of day-correlations for each station.

37 252 Step 4: Applying the soft thresholding denoising method to remove the noise in each of
38
39 253 the stacked cross-correlograms.

42 254 After step 4, we get the final EGFs for a pair of station, which can then be used to
43
44 255 measure group and phase velocity (Liu et al., 2019) or to do full waveform tomography (Yang &
45
46 256 Langston, 2019) to determine earth structure.

49 257

51 258

54 259

1
2
3 260**RESULTS**

4
5 261 We first apply the designating algorithm to “synthetic” seismic data constructed from real
6
7
8 262 data. The whole designating procedure can be better examined and compared with the known
9
10 263 noise input signal. Next, the entire flow will be applied to our subset of the TA array data and
11
12 264 compared with results from using TDN.

13
14 265 In our implementation of the CWT, we use the Morlet wavelet as the mother wavelet
15
16 266 $\psi(t)$ in equation (1) and (3) with 16 voices per octave. The designating method is not sensitive
17
18 267 to the number of the decomposition levels and smaller scale numbers will speed up the whole
19
20 268 processing (Mousavi and Langston, 2016). Using 16 voices per octave in the processing is large
21
22 269 enough for resolution while retaining efficiency. Choosing the right mother wavelet is also a
23
24 270 difficult task. Different target problems require different optimal wavelets. We tried a number of
25
26 271 different mother wavelets and by comparing the RMS error between the input noise and the final
27
28 272 designated results from the synthetic test, we achieve the least misfit using the Morlet wavelet.
29
30 273 Therefore, we will use the Morlet wavelet in our data processing.

31
32
33 274**Synthetic Data**

34
35
36 275
37
38 276 To best simulate real data, we construct a synthetic time series by using two segments of
39
40
41 277 recorded seismograms at station U41A. One segment contains 3,000 seconds of ambient noise
42
43 278 data. The other seismogram segment is with the same length but contains a teleseismic event.
44
45 279 The ambient noise segment is chosen to make sure that there is no earthquake or other obvious
46
47 280 transient signal in the selected time period by looking at the seismogram in the time domain and
48
49 281 the scalogram in the CWT domain. A teleseismic event occurred on July 25, 2012, was recorded
50
51 282 by the station and is used as the earthquake input. The soft thresholding denoising algorithm is
52
53
54
55
56
57
58
59
60

Processing Seismic Ambient Noise Data with the CWT

1
2
3 283 first applied on the earthquake segment to remove any ambient noise contained in the
4
5 284 seismogram. Then, both the ambient noise segment and the denoised earthquake segment are
6
7
8 285 filtered with a 1Hz low-pass filter. The earthquake segment is then tapered before the first arrival
9
10 286 time and at 1400 seconds to make sure there is no noise or signal before or after. The ambient
11
12 287 noise segment and the teleseismic event segment are then summed to produce the final synthetic
13
14
15 288 data (Fig. 3). Fig.3

16
17 289 The CWT spectrum of the synthetic data is calculated and shown in Fig. 3(d). The
18
19 290 earthquake and ambient noise are clearly distinguished and are indicated in the spectrum. The
20
21 291 CWT spectrum for ambient noise only falls into a specific range of scales and keeps a very stable
22
23 292 amplitude pattern. These scales correspond to the main frequency band of the ambient noise. The
24
25 293 earthquake contains signals over a wider range of scales which corresponding higher scale or
26
27 294 lower frequency data and with much larger amplitude. The CWT spectrum for the earthquake is
28
29 295 also changing with time and the pattern looks irregular. The overlapping scale band between the
30
31 296 earthquake data and the ambient noise data makes it impossible to separate them by just using a
32
33 297 bandpass filter.

34
35
36
37 298 After 1500 seconds, the seismogram is pure ambient noise and we use this segment to
38
39 299 calculate the ECDF of the ambient noise and estimate the noise level for each scale. After
40
41 300 obtaining the statistical properties of the ambient noise, we will decide whether the CWT
42
43 301 spectrum is kept the same or modified by using the criteria in equation (10). The CWT spectrum
44
45 302 after soft thresholding and the final designaled seismogram are shown in Figs 3e and f. The
46
47 303 designaling algorithm removes most of the earthquake signal and the noise superficially looks
48
49 304 the same before and after designaling. The time series after designaling looks more like the
50
51 305 original ambient noise since it has a balanced amplitude throughout. A comparison of particular
52
53
54
55
56
57
58
59
60

Processing Seismic Ambient Noise Data with the CWT

1
2
3 306 time windows before and after designating is also shown in Figs 3g and h. Noise is not modified
4
5 307 by this algorithm and appears qualitatively the same before and after designating. The CWT
6
7 308 spectrum of the designated time series is like a clipped version of the original spectrum which
8
9
10 309 suggests that there is still some small effects of the teleseism in the time series. We compare the
11
12 310 Fourier amplitude spectrum of input noise, input synthetic data and final designated results (Fig.
13
14 311 4). The designated time series has a slightly larger amplitude spectrum than the original spectrum
15
16
17 312 of the input noise due to the existence of some signals. But overall, the designated result shows
18
19 313 very good amplitude recovery.
20

Fig. 4

21 314

315 Real Data

26 316 All of data recorded by the selected TA stations during July 2012 are used as input data
27
28 317 to test the new processing flow. We will use the station V44A (Fig. 2) which is located within
29
30 318 the NMSZ as an example to show the results. There are plenty of earthquakes and transient
31
32 319 signals appearing in the original recording (Fig. 5), which make it perfect to test the new
33
34
35 320 processing flow. For comparison, we also process the same data with TDN as a benchmark.

Fig. 5

38 321 Station V44A and S38A are used to show the details of each processing step (Fig. 6). A
39
40 322 teleseismic event is obviously present in these particular data. Ambient noise is barely seen and
41
42 323 is buried beneath the earthquake signals. Earthquake signals are efficiently removed after soft
43
44 324 threshold designating and we get an amplitude-stable time series. Both stations show similar
45
46
47 325 results and no obvious earthquakes or transient signals are seen in the data after designating.

Fig. 6

49 326 The designated data are then correlated. The cross-correlogram from the soft thresholding
50
51 327 designated data has higher SNR compared with the one from TDN. The Rayleigh wave at
52
53
54 328 positive time lags is not clearly seen in the result using TDN. The running absolute mean
55
56
57
58
59
60

Processing Seismic Ambient Noise Data with the CWT

1
2
3 329 normalization method will only balance the amplitude of the original data to match the amplitude
4
5 330 of the ambient noise. However, the spectrum is dominated by the truncation of peaks and troughs
6
7
8 331 of the high amplitude signal in the time domain that non-linearly increases its high frequency
9
10 332 parts. Truncating the CWT is less severe because individual wavelets are intrinsically smooth
11
12 333 and are smoothed yet again during the inverse transform integration. The data of the two
13
14 334 stations for other days are processed in the same way and the final one-month stacked cross-
15
16
17 335 correlogram calculated from our processing flow also shows higher SNR (Fig. 6d). The
18
19 336 designating method removes earthquakes and other transient signals in a physical meaningful
20
21 337 way and it does not touch any ambient noise data. TDN achieves temporal normalization but
22
23
24 338 modifies the ambient noise while using a relatively harsh way to balance the amplitude of the
25
26 339 whole time series. We suggest that CWT designating preserves more of the noise characteristics
27
28 340 within the event time window.

30
31 341 After correlation and stacking, random noise is still clearly seen in the stacked EGF. To
32
33 342 further increase the SNR, we apply soft threshold denoising on the stacked EGF (Fig. 6e). This
34
35 343 will remove much of the noise within the final stacked cross-correlogram and give us an even
36
37 344 higher SNR result.

38
39
40 345 A more dramatic example is shown in Fig. 7. One-month correlation results are stacked
41
42 346 for stations W42A and W46A to get the EGF. Fourier filtering and the soft threshold denoising
43
44 347 method are applied to improve the SNR of the stacked EGF. The noise frequency range overlaps
45
46
47 348 with the signal frequency range. After the low-pass filter, noise is still obvious in the EGF and
48
49 349 the SNR does not increase significantly. However, with the soft threshold denoising method, the
50
51 350 noise is removed and the denoised EGF has a very high SNR, which provides for better input in
52
53
54 351 later processing steps, such as group and phase velocity extraction.

Fig. 7

1
2
3 352 Fig. 8 shows a record section of final EGFs for master station V44A from our processing
4
5 353 flow and TDN. Both processing flows give clear EGFs. Symmetric Rayleigh waves are also
6
7
8 354 observed. To better compare the two processing flows quantitatively, we compute the SNR by
9
10 355 using the ratio of maximum amplitude between -200s and 200s and the maximum amplitude for
11
12 356 the rest of data. Our new processing flow gives five to ten times higher SNR over using TDN.
13
14
15 357 Rayleigh waves are clearly observed on both positive and negative time lags with smaller
16
17 358 amplitude noise in between.

Fig. 8

19 359 The next step after acquiring the final EGFs is to calculate phase or group velocities
20
21 360 between each station pair. Although this is not the primary purpose of this paper, it is useful to
22
23 361 examine the differences in results obtained using the two data processing schemes. Readers may
24
25 362 refer to other studies and reports (e.g. Yao et al., 2006; Bensen et al., 2007) for more details of
26
27
28 363 dispersion calculation. Here, we show a comparison of the group velocities determined from
29
30 364 EGFs between the two processing flows for one station pair (Fig. 9). We calculated the group
31
32
33 365 velocity dispersion curve for station S38A using frequency-time analysis (Dziewonski et al.,
34
35 366 1969). Although group velocities have significant overlap between the two methods, they clearly
36
37 367 have different trends for periods greater than 15s. It is likely that these changes in the dispersion
38
39
40 368 curves will give rise to differences in the resulting velocity models.

Fig. 9

DISCUSSION

42 369
43
44 370
45
46 371 When deciding which processing flow to use for a specific dataset, we should observe
47
48 372 how many earthquakes and other transient signals are contained in the data. In the interest of
49
50 373 computational efficiency, if there are few transient events then CWT desingaling may be
51
52 374 overkill, wasting valuable compute cycles.
53
54
55
56
57
58
59
60

Processing Seismic Ambient Noise Data with the CWT

1
2
3 375 The new processing flow will deliver reliable and high SNR EGFs, which will be very
4
5 376 helpful in further processing steps, such as studying the attenuation or extracting body waves
6
7 377 from ambient noise seismic interferometry. However, some drawbacks of our processing flow
8
9 378 still need to be considered. The main concern is its relatively high computational cost. The CWT
10
11 379 is the most time-consuming part, which requires many forward and inverse Fourier transforms.
12
13 380 When processing large datasets such as years of ambient noise recording from large networks,
14
15 381 the computational time to designal will not be insignificant. Based on our processing experience,
16
17 382 it will take about half a minute to designal one-day of data for one station on a Macbook Pro
18
19 383 laptop. One possible solution is to use graphic processor unit (GPU) to calculate the wavelet
20
21 384 transform and remove the signals when processing large amounts of data, which will speed up
22
23 385 the processing significantly. It will take about 8 seconds to designal one-day of data for all 55
24
25 386 stations on a NVIDIA V100 GPU. Another possibility is to check the data first and only apply the
26
27 387 soft threshold designaling if signals are observed in the data. In this study, we only processed
28
29 388 one-month of data at 55 stations and the time for the processing is acceptable.
30
31
32
33
34

35 389 Another assumption for this method is that the ambient noise time series should be stable
36
37 390 in that its statistical properties should not change significantly in each one-day data segment. If
38
39 391 such changes are observed in the data, the largest noise level should be used in the designaling
40
41 392 process to avoid accidentally removing any ambient noise.
42
43
44

45 393 Ambient noise tomography has been widely used during the last 15 years and will be
46
47 394 continuously developed in the future. Acquiring more reliable EGFs and getting more
48
49 395 information from seismic interferometry will make this method more powerful and robust.
50

51 396
52
53
54 397
55
56
57
58
59
60

CONCLUSIONS

398
399 We propose a new ambient noise data processing flow to compute reliable EGFs. The
400 denoising and desIGNALING algorithm is based on the CWT with soft thresholding and is essential
401 to this flow. The whole processing flow is automated without any manual interference. The new
402 processing flow is suitable for data containing regional and teleseismic events or other transient
403 signals. The whole processing flow is divided into four steps: (1) single station data preparation,
404 (2) remove earthquakes and other transient signals in the seismic record, (3) spectrum whitening,
405 cross-correlation and temporal stacking, (4) remove the noise in stacked cross-correlogram to
406 deliver the final EGFs. The final EGFs can be used to extract phase or group velocity or to invert
407 for velocity structure by full waveform tomography.

408 The principal step during data preparation is to acquire pure ambient noise that is free of
409 earthquake and other transient signals (instrument irregularities and non-stationary noise sources
410 near to stations, etc.). We adopt a method based on the CWT to remove these unwanted signals.
411 The intrinsic time-frequency property of the CWT makes it possible to isolate noise and signal
412 efficiently. A segment of pure ambient noise is usually obtainable and can be used to estimate
413 the statistical property of the noise in the CWT domain. The estimated noise statistical properties
414 are then used as a guide to detect whether the data point at different time and scales in the CWT
415 domain is noise or not. A soft thresholding method is used to remove the signal if the data
416 exceeds the noise level. We constructed synthetic data based on recorded noise and an
417 earthquake to successfully test the method. Use on more extensive data shows excellent signal
418 removal. Other denoising algorithms based on the CWT such as block thresholding (Mousavi et
419 al., 2016) could also be used to remove earthquakes and other signals in the time series but they
420 also require much more computational cost. Our method is efficient for large datasets.

Processing Seismic Ambient Noise Data with the CWT

1
2
3 421 The denoising method can also be used to remove the noise in the final EGFs to further
4
5 422 increase the SNR. We use the same algorithm as in the designating step but in a reverse manner
6
7
8 423 to significantly increase the SNR in the final EGF. This denoising method performs better than
9
10 424 bandpass filters since a Fourier filter has no time resolution.

11
12 425 We applied our processing flow to one-month of data from EarthScope TA stations near
13
14 426 the NMSZ. Many earthquakes and other transient signals were recorded by the stations which
15
16
17 427 make this dataset an appropriate test dataset for the algorithm. We obtain better EGFs with
18
19 428 higher SNR than results using TDN. Except for removing earthquake and other transient signals
20
21 429 that obscure the ambient noise data, and noise removal for the final stacked empirical Green's
22
23 430 function, our processing flow is basically the same as previously proposed (Bensen et al., 2007).
24
25
26 431 In regions where few earthquakes occur, there should not be many differences in the resulting
27
28 432 EGFs between these two processing flows. However, the stacked EGF denoising step is
29
30 433 recommended for both methods because it has relatively low computational cost but dramatically
31
32 434 increases the SNR.

33 435

34 436 **DATA AND RESOURCES**

35
36
37
38 437 Seismogram data used in this study are collected from IRIS (<http://www.iris.edu>, last
39
40 438 accessed on January 2019). A MATLAB GUI code to process simple dataset and visualize the
41
42 439 results from the CWT denoising and designating method used in this study can be accessed at
43
44
45 440 <http://www.ceri.memphis.edu/people/clangstn/software.html> (last accessed on August 2019).
46
47
48 441 A CPU/GPU code to process large ambient noise datasets can be downloaded from
49
50 442 https://github.com/SwiftHickory/bc_denoise.git (last accessed on August 2019).
51
52
53

54 443

1
2
3 444**ACKNOWLEDGEMENT**4
5 445

We are grateful for financial support from the Center for Earthquake Research and

6
7 446

Information to perform this research. This research was supported by the Air Force Research

8
9 447

Laboratory under contract FA9453-18-C-0064.

10
11 44812
13 449**REFERENCE**14
15 450

Ansari, A., Noorzad, A., Zafarani, H. & Vahidifard, H., 2010. Correction of highly noisy strong

16
17 451

motion records using a modified wavelet denoising method, *Soil Dynam. Earthq. Eng.*,

18
19 452

30, 1168–1181.

20
21 453

Beenamol, M., Prabavathy, S. & Mohanalin J., 2012. Wavelet based seismic signal de-noising

22
23 454

using Shannon and Tsallis entropy, *Comput. Math. Appl.*, 64, 3580–3593.

24
25 455

Bensen, G. D., Ritzwoller, M. H., & Shapiro, N. M., 2008. Broadband ambient noise surface

26
27 456

wave tomography across the United States, *J. Geophys. Res.*, 113(B5).

28
29 457

Bensen, G. D., Ritzwoller, M. H., Barmin, M. P., Levshin, A. L., Lin, F., Moschetti, M. P., ... &

30
31 458

Yang, Y., 2007. Processing seismic ambient noise data to obtain reliable broadband

32
33 459

surface wave dispersion measurements, *Geophys. J. Int.*, 169(3), 1239-1260.

34
35 460

Chik, Z., Islam, T., Rosyidi, S. A., Sanusi, H., Taha, M. R. & Mustafa, M. M., 2009. Comparing

36
37 461

the performance of Fourier decomposition and wavelet decomposition for seismic signal

38
39 462

analysis, *Eur. J. Scientif. Res.*, 32, 314–328.

40
41 463

Cox, R. T., Van Arsdale, R. B. & Harris, J. B., 2001. Identification of possible Quaternary

42
43 464

deformation in the northeastern Mississippi Embayment using quantitative geomorphic

44
45 465

analysis of drainage-basin asymmetry, *Geol. Soc. Am. Bull.*, 113(5), 615-624.

Processing Seismic Ambient Noise Data with the CWT

- 1
2
3 466 Daubechies, I., 1992. Ten Lectures on Wavelets, Vol. 61, SIAM, Philadelphia, Pennsylvania,
4
5 467 357 pp., doi: 10.1137/1.9781611970104.
6
7
8 468 Dunn, M., DeShon, H. R., & Powell, C. A., 2013. Imaging the New Madrid seismic zone using
9
10 469 double-difference tomography, *J. Geophys. Res.*, 118(10), 5404-5416.
11
12 470 Dziewonski, A.M., Bloch, S. & Landisman, M., 1969. A technique for the analysis of transient
13
14 471 seismic signals, *Bull. Seism. Soc. Am.*, 59, 427– 444.
15
16
17 472 Elad, M., & Aharon, M., 2006. Image denoising via sparse and redundant representations over
18
19 473 learned dictionaries, *IEEE Trans. Image Process.*, 15, 3736–3745.
20
21
22 474 Emry, E. L., Shen, Y., Nyblade, A. A., Flinders, A. & Bao, X., 2018. Upper Mantle Earth
23
24 475 Structure in Africa From Full-Wave Ambient Noise Tomography, *Geochemistry,*
25
26 476 *Geophysics, Geosystems*, 20(1), 120-147.
27
28
29 477 Farge, M., 1992. Wavelet transforms and their applications to turbulence, *Annu. Rev. Fluid*
30
31 478 *Mech.*, 24, 395–458, doi: 10.1146/annurev.fl.24.010192.002143.
32
33
34 479 Gao, H., & Shen, Y., 2014. Upper mantle structure of the Cascades from full-wave ambient noise
35
36 480 tomography: Evidence for 3D mantle upwelling in the back-arc, *Earth and Planetary*
37
38 481 *Science Letters*, 390, 222-233.
39
40
41 482 Hildenbrand, T. G., 1985. Rift structure of the northern Mississippi embayment from the analysis
42
43 483 of gravity and magnetic data, *J. Geophys. Res.*, 90(B14), 12607-12622.
44
45
46
47 484 Johnston, A. C., & Schweig E. S., 1996. The enigma of the New Madrid earthquakes of 1811-
48
49 485 1812, *Anna. Rev. Earth Planet. Scie.*, 24, 339-384.
50
51
52
53
54
55
56
57
58
59
60

Processing Seismic Ambient Noise Data with the CWT

- 1
2
3 486 Langston, C. A., & Mousavi, S. M., 2019. Separating signal from noise and from other signal
4
5 487 using non-linear thresholding and scale-time windowing of continuous wavelet
6
7 488 transform, *Bull. Seism. Soc. Am.*, accepted for publication.
9
10 489 Langston, C. A., Chiu, S. C. C., Lawrence, Z., Bodin, P., & Horton, S., 2009. Array observations
11
12 490 of microseismic noise and the nature of H/V in the Mississippi embayment, *Bulletin of*
13
14 491 *the Seismological Society of America*, 99(5), 2893-2911.
16
17 492 Lecocq, T., Caudron, C. & Brenguier, F., 2014. MSNoise, a python package for monitoring
18
19 493 seismic velocity changes using ambient seismic noise, *Seismological Research*
20
21 494 *Letters*, 85(3), 715-726.
23
24 495 Liang, C., & Langston C. A., 2008. Ambient seismic noise tomography and structure of eastern
25
26 496 North America. *J. Geophys. Res.*, 113(B3).
28
29 497 Lin, F. C., Moschetti, M. P. & Ritzwoller, M. H., 2008. Surface wave tomography of the western
30
31 498 United States from ambient seismic noise: Rayleigh and Love wave phase velocity
32
33 499 maps, *Geophys. J. Int.*, 173(1), 281-298.
35
36 500 Liu, C., Langston, C. A. & Powell C. A., 2019. Crustal and uppermost mantle shear wave
37
38 501 velocity and radial anisotropy beneath the Mississippi embayment from ambient noise
39
40 502 tomography, manuscript submitted for publication.
42
43 503 Mousavi, S. M. & Langston, C. A., 2016, Hybrid Seismic Denoising Using Higher-Order
44
45 504 Statistics and Improved Wavelet Block Thresholding, *Bull. Seismol. Soc. Am.*, 106(4),
46
47 505 1380-1393.
48
49
50
51
52
53
54
55
56
57
58
59
60

Processing Seismic Ambient Noise Data with the CWT

- 1
2
3 506 Mousavi, S. M., Langston, C. A. & Horton, S. P., 2016. Automatic micro-seismic denoising and
4
5 507 onset detection using the synchrosqueezed-con- tinuous wavelet transform, *Geophysics*,
6
7 508 81(4), 1–15, doi: 10.1190/ GEO2015-0598.1.
8
9
10 509 Nyamwandha, C. A., Powell, C. A. & Langston, C. A., 2016. A joint local and teleseismic
11
12 510 tomography study of the Mississippi Embayment and New Madrid Seismic Zone, *J.*
13
14 511 *Geophys. Res. B Solid Earth Planets*, 121(5), 3570-3585.
15
16
17 512 Pazos, A., Gonzalez, M. J. & Alguacil, G., 2003. Non-linear filter using the wavelet transform
18
19 513 applied to seismological records, *J. Seismol.*, 7, 413–429.
20
21
22 514 Powell, C. A., Withers, M. M., DeShon, H. R. & Dunn, M. M., 2010. Intrusions and anomalous
23
24 515 Vp/Vs ratios associated with the New Madrid seismic zone, *J. Geophys. Res. B Solid*
25
26 516 *Earth Planets*, 115(B8).
27
28
29 517 Rioul, O. & Duhamel, P., 1992. Fast algorithms for discrete and continuous wavelet
30
31 518 transforms, *IEEE transactions on information theory*, 38(2), 569-586.
32
33
34 519 Sabra, K. G., Gerstoft, P., Roux, P., Kuperman, W. A. & Fehler, M. C., 2005. Extracting time-
35
36 520 domain Green's function estimates from ambient seismic noise, *Geophysical Research*
37
38 521 *Letters*, 32(3).
39
40
41 522 Shapiro, N. M., Campillo, M., Stehly, L. & Ritzwoller, M. H., 2005. High-resolution surface-
42
43 523 wave tomography from ambient seismic noise, *Science*, 307(5715), 1615-1618.
44
45
46 524 Starck, J. L., Murtagh, F. & Fadili, J. M., 2010. *Sparse Image and Signal Processing*. New York:
47
48 525 Cambridge University Press.
49
50
51 526 Tary, J. B., Herrea, R. H., Han, J. & Baan, M. V. D., 2014. Spectral estimation—What is new?
52
53 527 What is next? *Rev. Geophys.*, 52(4), 723–749, doi: 10.1002/2014RG000461.
54
55
56
57
58
59
60

Processing Seismic Ambient Noise Data with the CWT

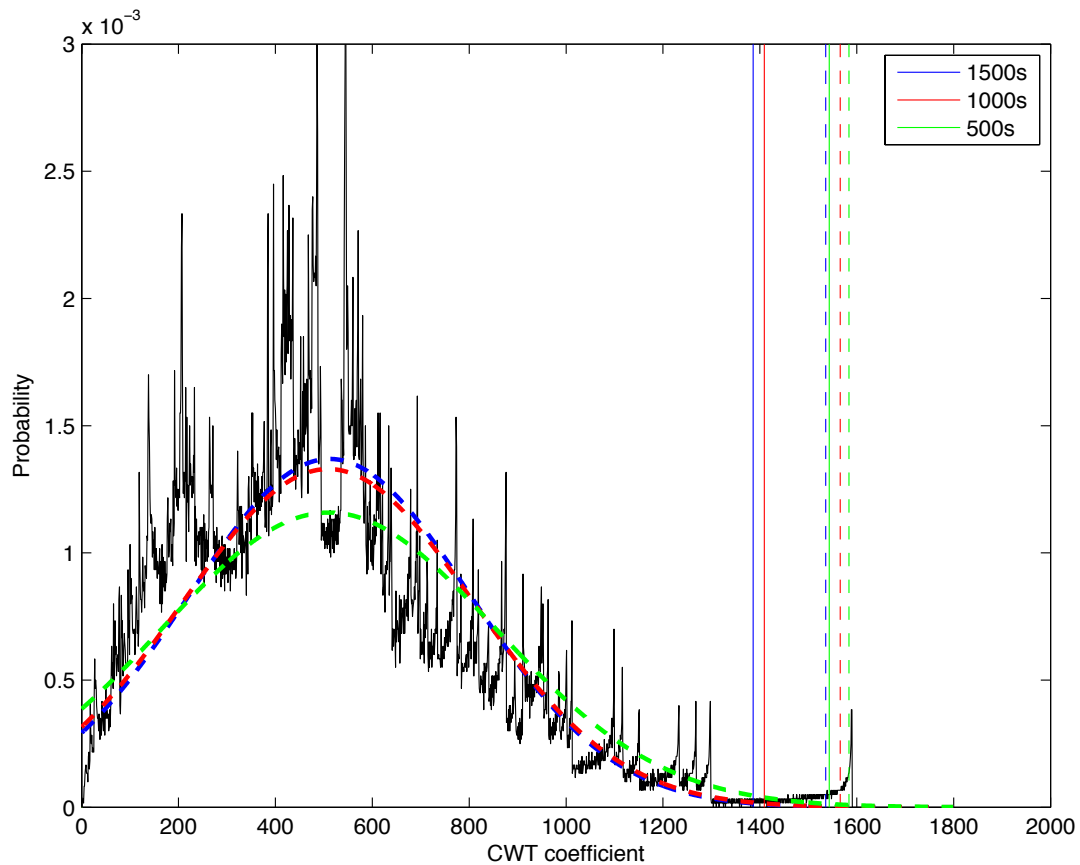
- 1
2
3 528 Thomas, W. A., 2006, Tectonic inheritance at a continental margin, *GSA today*, 16(2), 4-11.
4
5
6 529 To, C. A., Moore, J. R. & Glaser, S. D., 2009. Wavelet denoising techniques with applications to
7
8 530 experimental geophysical data, *Signal Process.*, 89, 144–160, doi:
9
10 531 10.1016/j.sigpro.2008.07.023.
11
12
13 532 Torrence, C. & Compo, G. P., 1998. "A practical guide to wavelet analysis." *Bulletin of the*
14
15 533 *American Meteorological Society*, 79(1), 61-78.
16
17
18 534 Tuttle, M. P., Schweig, E. S., Sims, J. D., Lafferty, R. H., Wolf, L. W. & Haynes, M. L., 2002.
19
20 535 The earthquake potential of the New Madrid seismic zone, *Bull. Seismol. Soc. Am.*,
21
22 536 92(6), 2080-2089.
23
24
25 537 Van Arsdale, R. & Cupples, W., 2013. Late Pliocene and Quaternary deformation of the Reelfoot
26
27 538 rift, *Geosphere*, 9(6), 1819-1831.
28
29
30 539 Van Arsdale, R., Bresnahan, R., McCallister, N. & Waldron, B., 2007. Upland Complex of the
31
32 540 central Mississippi River valley: Its origin, denudation, and possible role in reactivation
33
34 541 of the New Madrid seismic zone, *Geological Society of America Special Papers*, 425,
35
36 542 177-192.
37
38
39 543 Wapenaar, K. & Fokkema, J., 2006. Green's function representations for seismic
40
41 544 interferometry, *Geophysics*, 71(4), SI33-SI46.
42
43
44 545 Weaver, J. B., Yansun, X., Healy, D. M. & Cromwell, L. D., 1991. Filtering noise from images
45
46 546 with wavelet transforms, *Matnetic Resonance in Medicine*, 21, 288-295.
47
48
49 547 Yang, Y. & Langston, C. A., 2019. Full waveform ambient noise tomography for the northern
50
51 548 Mississippi embayment, unpublished manuscript.
52
53
54
55
56
57
58
59
60

Processing Seismic Ambient Noise Data with the CWT

- 1
2
3 549 Yao, H., van Der Hilst, R. D. & De Hoop, M. V., 2006. Surface-wave array tomography in SE
4
5 550 Tibet from ambient seismic noise and two-station analysis—I. Phase velocity
6
7 551 maps, *Geophys. J. Int.*, 166(2), 732-744.
8
9
10
11
12
13
14
15
16
17
18
19
20
21
22
23
24
25
26
27
28
29
30
31
32
33
34
35
36
37
38
39
40
41
42
43
44
45
46
47
48
49
50
51
52
53
54
55
56
57
58
59
60

552

FIGURES

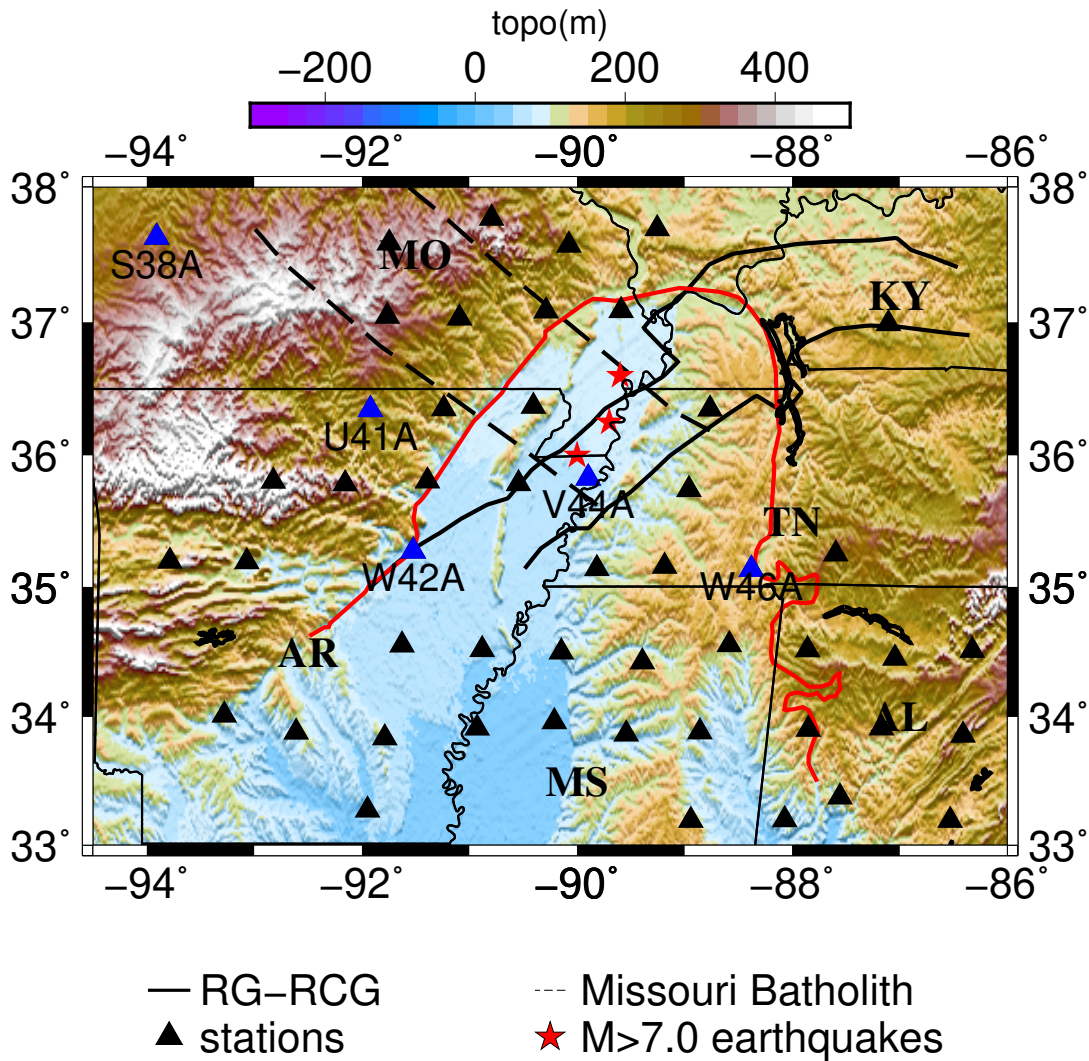


553

554 Figure 1. Empirical probability density function of the ambient noise CWT coefficients (black
 555 line) and the estimated probability density function (dashed line) with the assumption of normal
 556 distribution. The ambient noise data used for this plot are shown in the synthetic test figure. The
 557 empirical probability density function is plotted only with 1500s data and the noise level is
 558 estimated with different data length of 1500s, 1000s and 500s, respectively. The vertical solid
 559 line and dashed line show the estimated noise level based on Gaussian distribution and empirical
 560 probability distribution with 99% confidence value, respectively. Notice that the estimated noise
 561 level is more stable with ECDF method.

562

Processing Seismic Ambient Noise Data with the CWT



563

564 Figure 2. The distribution of the seismic stations used in this study (filled triangles).

565 Continuously seismic recordings during July 2012 from a subset of the USArray Transportable
 566 Array stations in and around the northern Mississippi embayment are our benchmark test dataset.

567 Major geological features include the Reelfoot Graben (RG), Rough Creek Graben (RCG) and

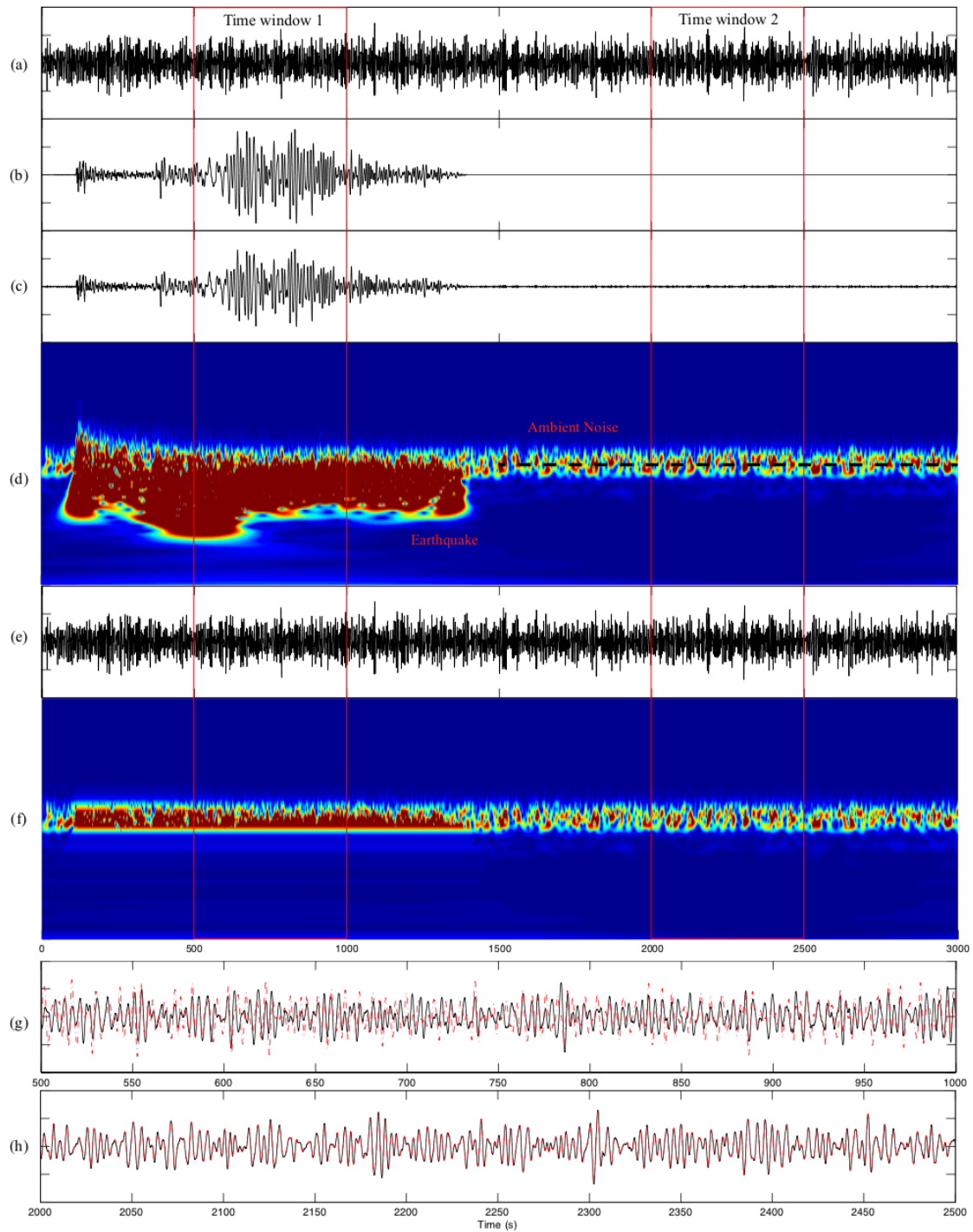
568 Missouri batholith (between two dashed lines). The boundary of the Mississippi embayment is

569 shown by the red lines. The locations of the three large earthquakes that occurred in 1811 and

570 1812 are shown as the red stars (Johnston & Schweg, 1996). Several specific stations used as

571 examples in the rest of this article are annotated.

572

Processing Seismic Ambient Noise Data with the CWT

573

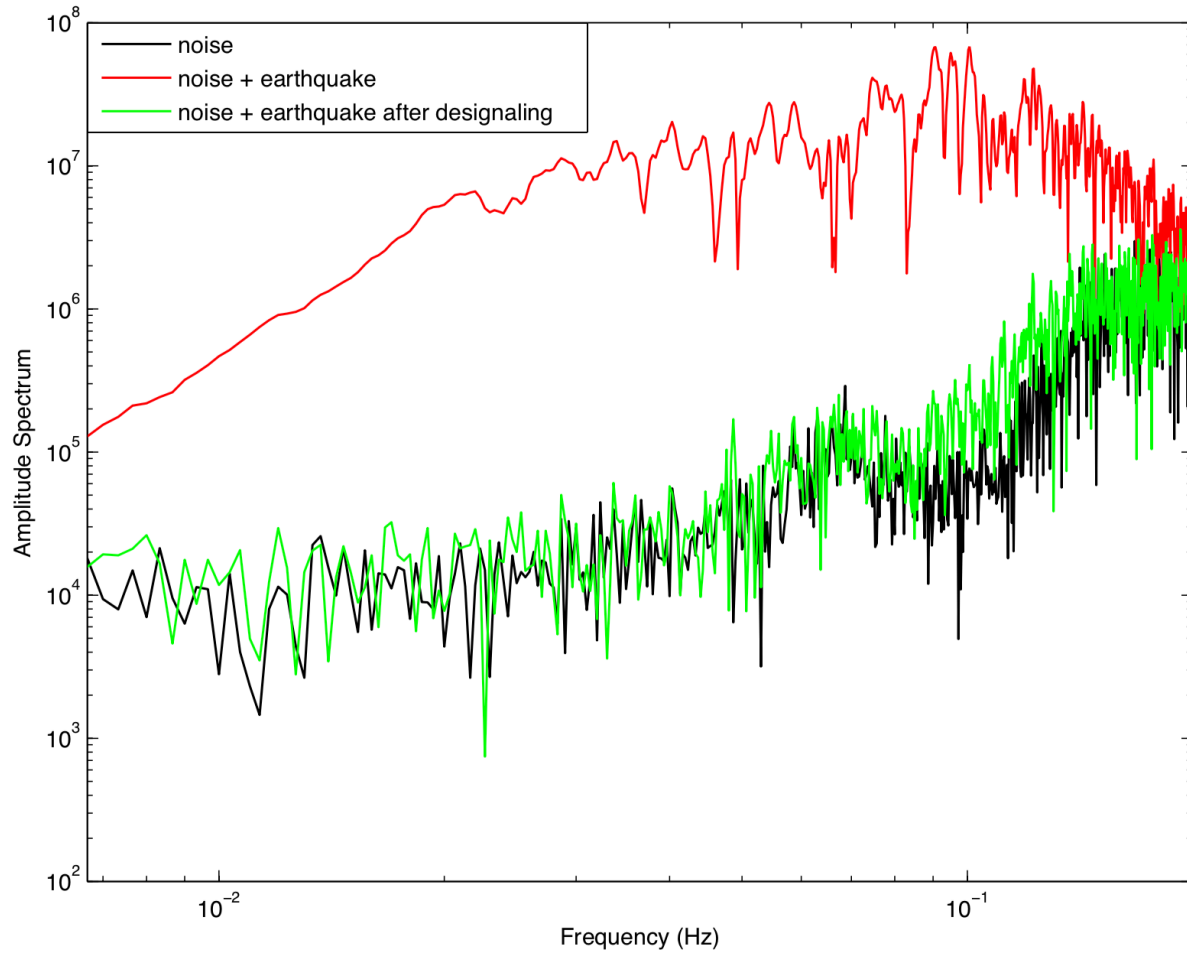
574 Figure 3. Designing synthetic test based on recorded ambient noise and earthquake data. (a)

575 3000s ambient noise data from station U41A. (b) The July 25, 2012, teleseismic earthquake

576 recorded by station U41A. The data are denoised with the CWT soft thresholding denoising

Processing Seismic Ambient Noise Data with the CWT

1
2
3 577 algorithm and a 1Hz low-pass filter is applied after denoising. Data before the first arrival and
4
5 578 after 1400 seconds are tapered. (c) Synthetic data constructed by summing ambient noise data in
6
7 579 (a) and seismic event data in (b). (d) The modulus of the complex CWT spectrum of synthetic
8
9 580 data in (c). The dashed line indicates the data used in (a). (e) Synthetic data after designating
10
11 581 shown in the time domain. (f) Synthetic data after designating shown in the CWT domain. (g)
12
13 582 The comparison of seismic data before designating (solid line) and after designating (dashed
14
15 583 line) with the data in the time window 1. (h) Same as (g) but for time the window 2. The vertical
16
17 584 red lines delineate the two 500s time windows.
18
19
20
21
22
23
24
25
26
27
28
29
30
31
32
33
34
35
36
37
38
39
40
41
42
43
44
45
46
47
48
49
50
51
52
53
54
55
56
57
58
59
60

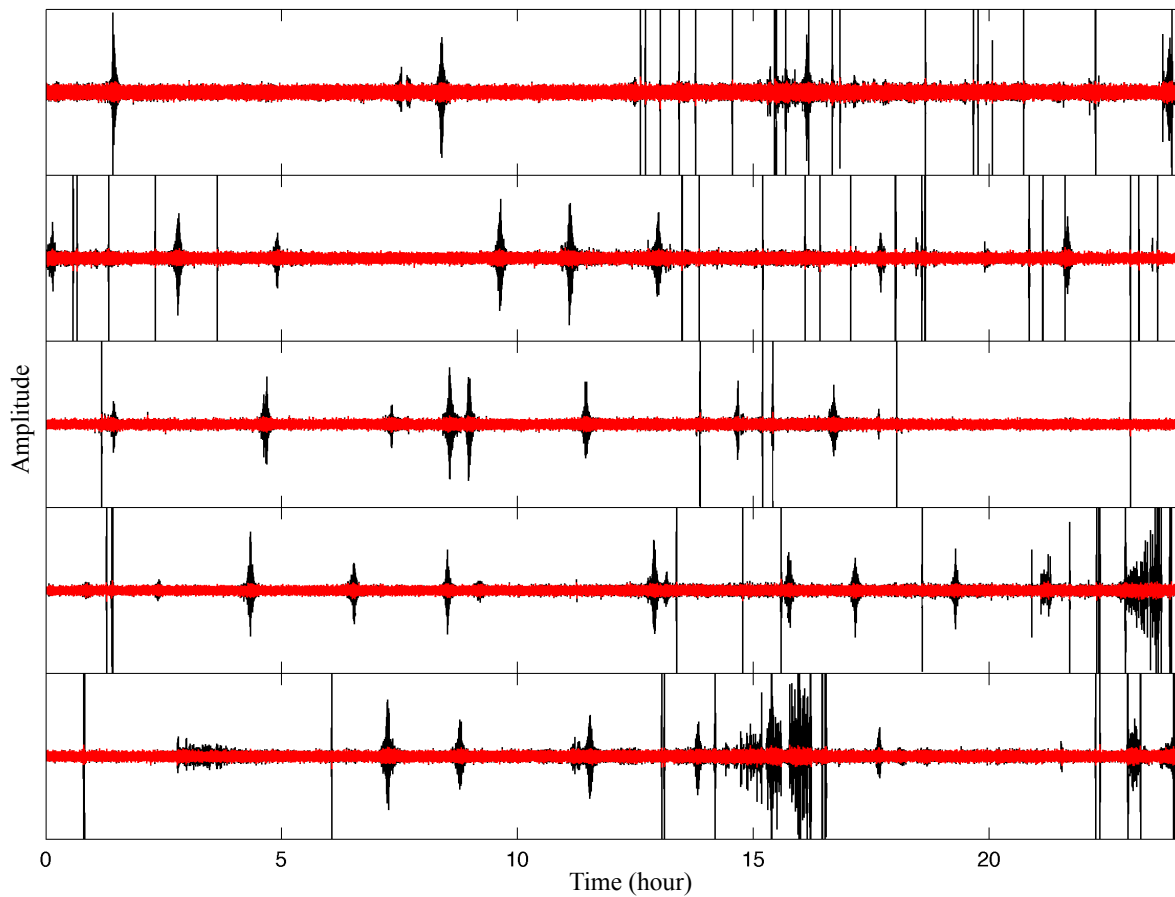


585

586 Figure 4. The comparison of the Fourier amplitude spectrum between the original noise data, the

587 noise data added with earthquake data and the final designaled data.

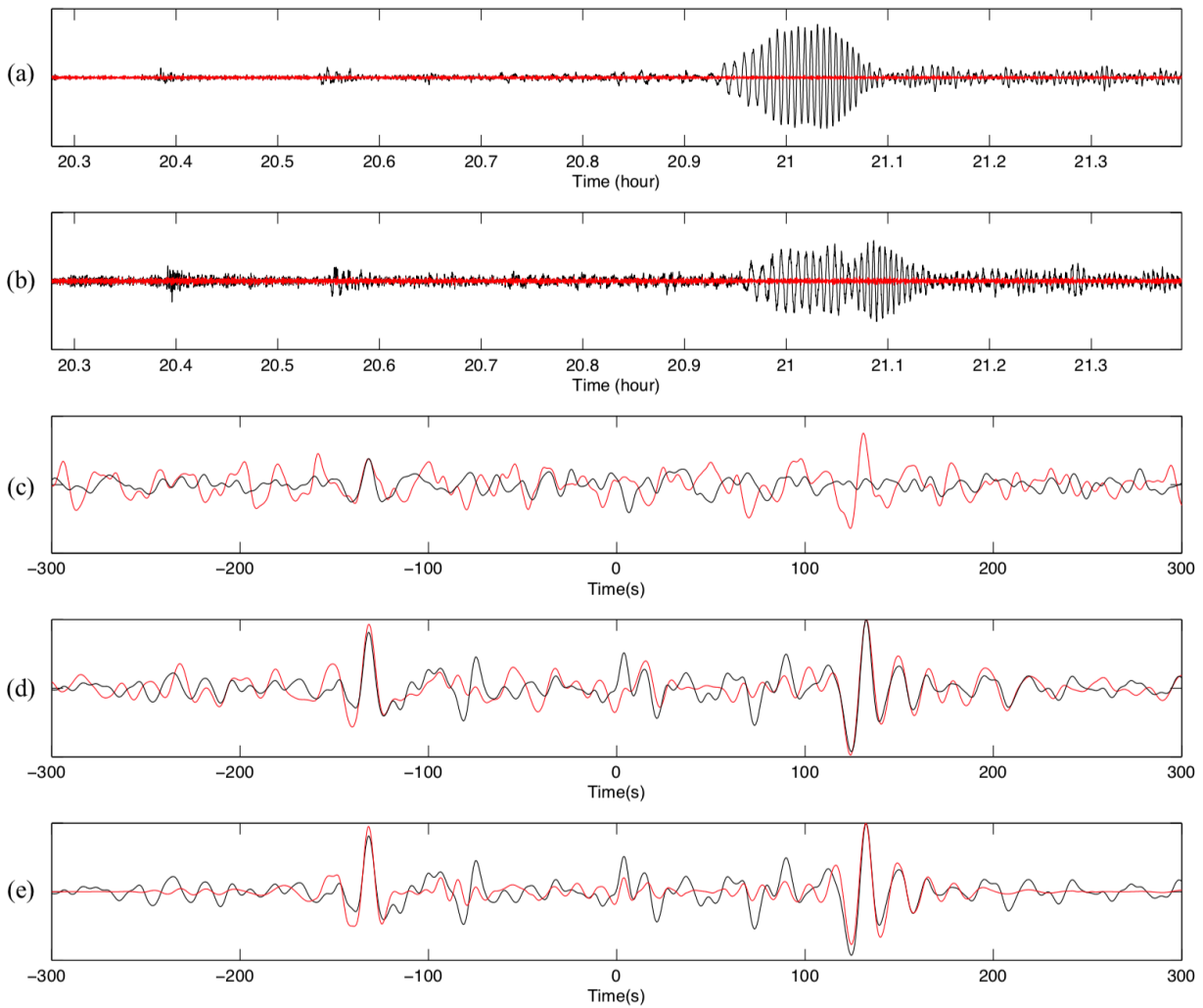
588

Processing Seismic Ambient Noise Data with the CWT

589

590 Figure 5. Vertical component seismograms of station V44A recorded during the first five-days of
591 July 2012 (black) and the designated result (red). Each row shows one-day of seismic data. There
592 are many earthquakes and transient signals recorded by the station. These signals are
593 successfully removed after designating.

594

Processing Seismic Ambient Noise Data with the CWT

595

596 Figure 6. EGF calculation between station V44A and S38A. (a) A segment of seismic record for

597 station S38A on July 28, 2012, with the black line indicating the original data and the red line

598 showing the designated results. A teleseismic event is seen within this time period and is

599 removed after designaling. (b) Same as (a) but for station V44A. (c) One-day cross-correlation

600 between station S38A and station V44A for date July 28, 2012, calculated using TDN (black)

601 and the designated data (red). (d) One-month stacked cross-correlogram obtained from TDN

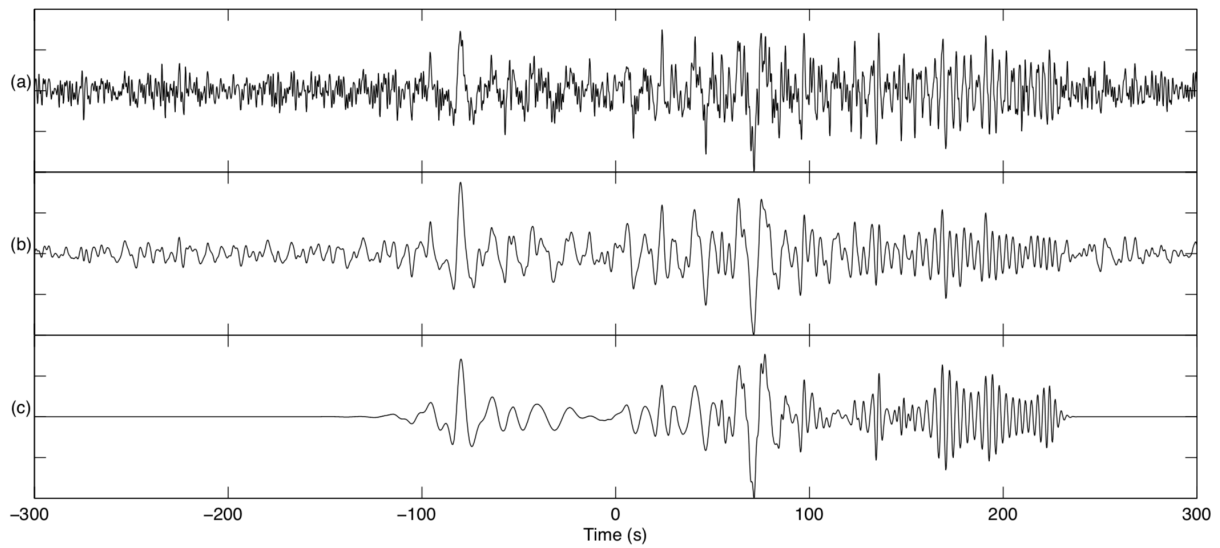
602 (black) and our processing flow before the final denoising step (red). (e) One-month stacked

603 cross-correlogram obtained from TDN and our processing after the final denoising step (red).

604 Absolute amplitude is plotted in (c). The amplitude is normalized in (d) and (e).

Processing Seismic Ambient Noise Data with the CWT

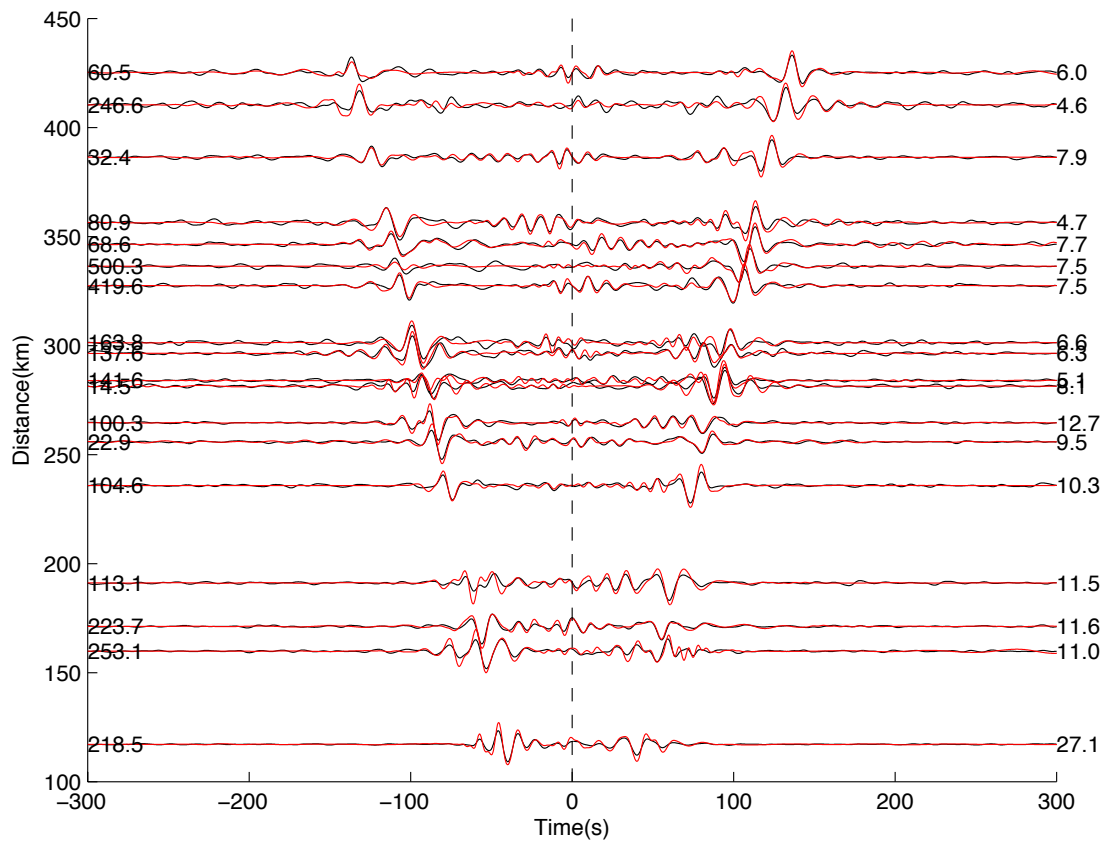
605



606

607 Figure 7. Application of soft threshold denoising on the final stacked cross-correlogram for
608 stations W42A and W46A. (a) Original stacked cross-correlogram. (b) Stacked cross-
609 correlogram with a 0.3Hz low-pass filtered applied. (c) Stacked cross-correlogram after soft
610 thresholding denoising.

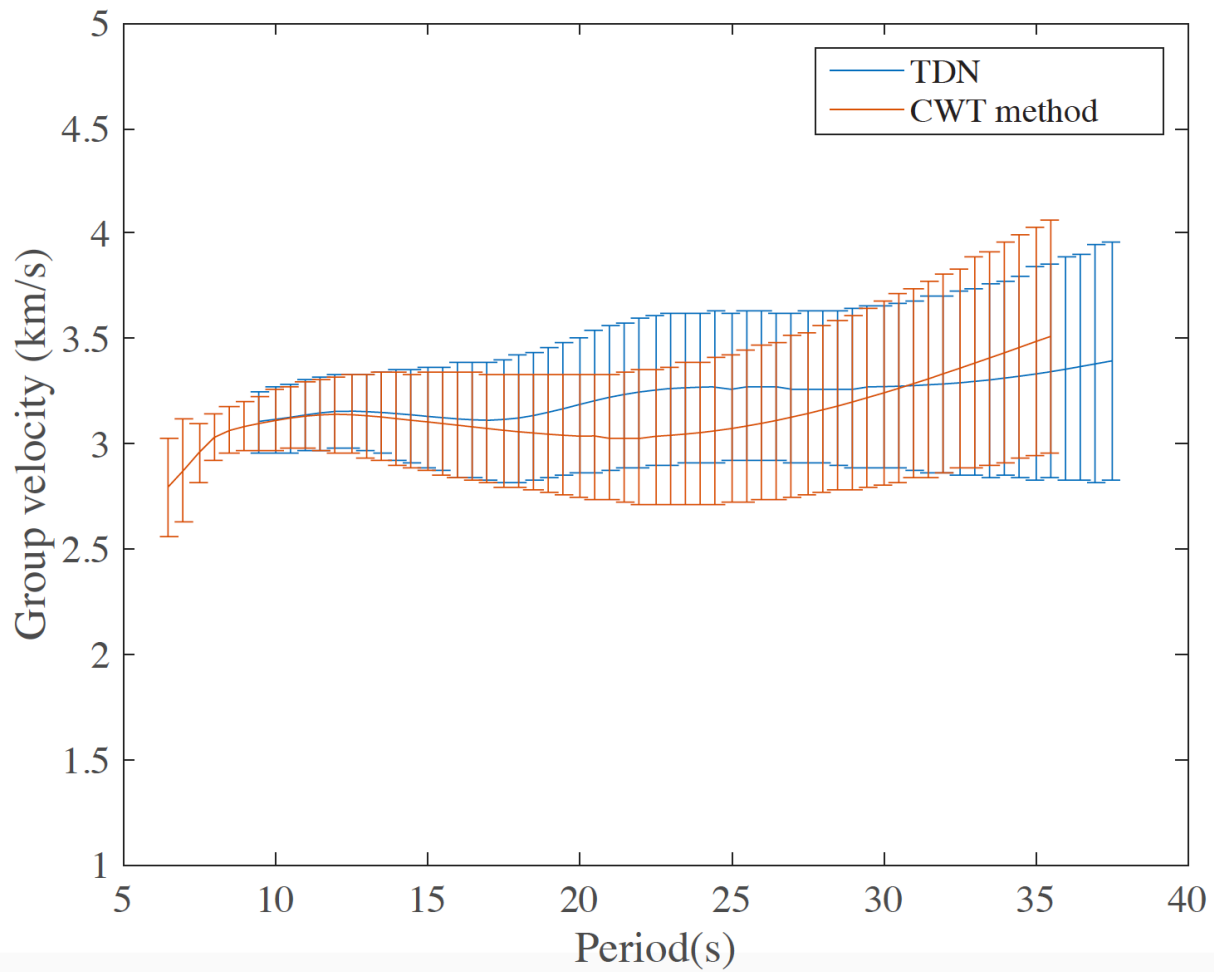
611

Processing Seismic Ambient Noise Data with the CWT

612

613 Figure 8. EGFs record section acquired from TDN (black) and our processing flow (red) for
 614 station V44A. SNR for the results from TDN is shown on the right side and for our method on
 615 the left side. The SNR is calculated using the ratio between the maximum amplitude from the
 616 time window -200s to 200s and maximum amplitude of the remaining part. A bandpass filter
 617 between 0.01s and 0.15s is applied to all data. The amplitude is the stacked absolute amplitude
 618 without normalization.

619

Processing Seismic Ambient Noise Data with the CWT

620

621 Figure 9. Comparison of group velocity dispersion curves from station V44A to station S38A

622 from an EGF using TDN (blue) and our processing flow (red).

623